Supplementary Information : Lava planet interior dynamics governs the long-term evolution of its magma ocean

Charles-Édouard Boukaré[1*], Daphné Lemasquerier[2], Nicolas B. Cowan[4,1], Henri Samuel[1] and James Badro[1]

[1*]Institut de Physique du Globe de Paris, 1, rue Jussieu, Paris, 75005, France.
[2*]University of St. Andrews, School of Mathematics and Statistics, North Haugh, St Andrews, KY16 9SS, UK.
[4*]Department of Earth and Planetary Sciences, McGill University, 3450, rue University, Montréal, H3A0E8, Canada.
[5*]Department of Physics, McGill University, 3450, rue University, Montréal, H3A0E8, Canada.

*Corresponding author(s). E-mail(s): boukare@ipgp.fr;
Contributing authors: d.lemasquerier@st-andrews.ac.uk; nicolas.cowan@mcgill.ca; badro@ipgp.fr; samuel@ipgp.fr;

Abstract

Keywords: Exoplanets, Magma Oceans, Rocky Planets Formation and Evolution, Atmosphere-interior interaction.

Parametrization

We use the following parametrization for the solid-liquid isochemical density constrast shown in Figure S1,

$$R_p(z) = \frac{R_p^s - R_p^c}{1 - e^{-\gamma}} \left(e^{-\gamma z} - 1\right) + R_p^s, \quad (1)$$

where z is the dimensionless depth, $R_p^s = 11.53$, $R_p^c = 0.82$, and $\gamma = 6$. The subscripts s and c refer to the surface and core-mantle-boundary (CMB), respectively.

We use the following parametrization for the compositional density constrast, i.e., that quantifies the role of the FeO content on density, shown in Figure S1,

$$R_c(z) = R_c^s + z \times (R_c^c - R_c^s), \quad (2)$$

where z is the dimensionless depth, $R_c^s = 4.11$, $R_c^c = 12.35$.

The branches that describe the liquidus and solidus temperatures in the simplified phase diagram we use (Fig. S2) are parameterized as follows,

$$T_L(z) = T_{\mathrm{FeO}}(z) + (T_{\mathrm{MgO}}(z) - T_{\mathrm{FeO}}(z))\,(1 - x_l^m)\,, \quad (3)$$

$$T_S(z) = T_{\mathrm{FeO}}(z) + (T_{\mathrm{MgO}}(z) - T_{\mathrm{FeO}}(z))\,(1 - x_s)^n \quad (4)$$

where T_L is the liquidus temperature, T_S is the solidus temperature, T_{MgO} and T_{FeO} are the melting temperature of the pure end-members, x_l is the composition of the liquid in FeO, x_s is the composition of the solid in FeO, m and n are constant that we used to adjust the shape of the loop. We assume that T_{FeO} and T_{MgO} vary linearly with depth. In the dimensionless form, we use $T_{FeO}^s = 0.31$, $T_{FeO}^c = 0.44$, $T_{MgO}^s = 0.57$, $T_{MgO}^c = 0.88$, $m = 1.7$, and n= 1.1.

Physical parameters

The physical parameters used in the 2D multiphase fluid dynamics simulations are listed in Tables 4. The physical parameters used in the 3D spherical simulations are listed in Table S2.

Comparison of 2D vs. 3D approaches

We use the 3D spherical simulations to validate our 2D Cartesian approach when the magma ocean is global. In particular, our 2D multiphase model considers an infinite Prandtl number dynamics, a regime representative of mantle-like convection with important viscous effects and negligible inertia. In the fully-molten period, if the viscosity of the fluid is low enough, finite Prandtl number dynamics becomes more relevant. Because of reduced viscous effects, the dynamics would be turbulent, and possibly affected by rotation, as suggested for the early Earth's magma ocean [8, 9]. Fig. S3 shows that even in the

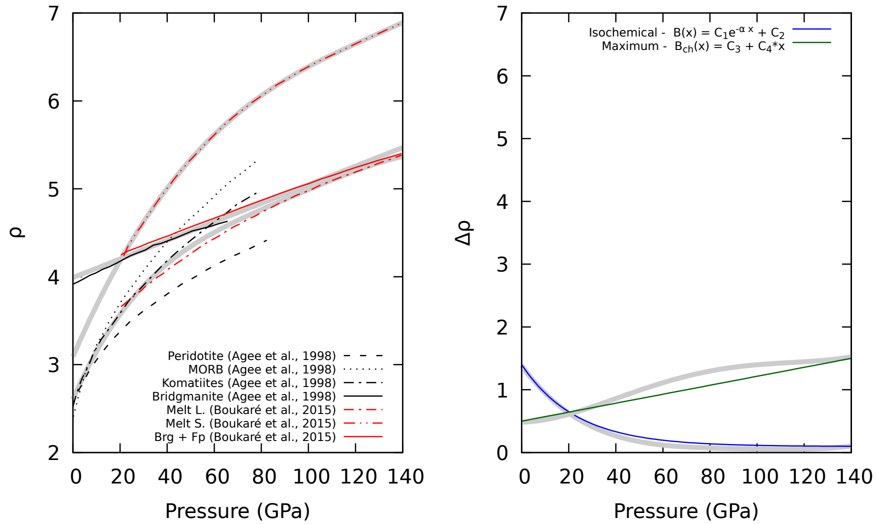

Fig. S1 Density contrast parametrization. (Left) Density of solid and liquid silicate as function of pressure for various composition. (Right) Density difference between solid and liquid. The thick grey lines correspond to the exact difference between the density curves shown on the left. The color lines depict the parametrization used in this study. The isochemical density contrast is shown in blue and captures to the effect of highest compressibility of silicate melt compared to their solid counterparts. The chemical density contrast corresponds to the density contrast between iron-rich and iron-free silicates.

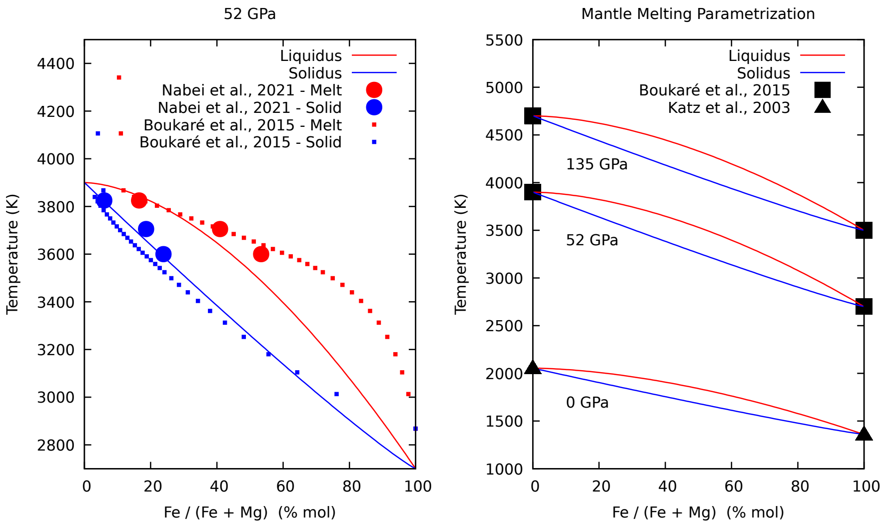

Fig. S2 Idealized binary loop model used to model solid-liquid melting relations in the Earth's mantle. This parameterization was obtained by fitting diamond anvil cell experiments [1] and self-consistent thermodynamic calculations [2].

Parameters	Symbol (unit)	Value
Mean density	ρ_0 (kg m^{-3})	4500
Depth-dependent isochemical density contrast	- (kg m^{-3})	1400 – 100
Depth-dependent compositional density contrast	- (kg m^{-3})	500 – 1500
Thermal expansivity	α_0 (K^{-1})	10^{-5}
Gravity acceleration	g_0 (m s^{-2})	9.81
Magma ocean thickness	D (km)	3000
Thermal diffusivity	κ (m^2 s^{-1})	10^{-6}
Thermal capacity	C_P (J K^{-1} kg^{-1})	1000
Latent heat of solidification	L(J kg^{-1})	1000
Solid viscosity	η_s (Pa s)	10^{22}
Liquid viscosity	η_l (Pa s)	10^{0}
Compaction viscosity	η_b (Pa s)	10^{22}
Crystal size[1]	a (m)	10^{-6}-10^{-2}
Surface temperature at the sub-stellar point	- (K)	2700
Surface temperature at the anti-stellar point	- (K)	0
Core temperature	- (K)	5000
Adiabatic temperature increase over the MO thickness	- (K)	1800
Maximum super adiabatic vertical temperature difference	ΔT_m (K)	2700
Maximum super adiabatic horizontal temperature difference	ΔT_h (K)	2700
Dimensionless parameters (Lava Planet)		
Solid-state Rayleigh	Ra	3.22×10^{6}
Liquid-state thermal Rayleigh	-	3.22×10^{28}
Solid-liquid viscosity contrast	-	10^{22}
Depth-dependent isochemical density contrast	R_p	11.15 – 0.823
Depth-dependent compositional density contrast	R_c	4.15 – 12.34
Stefan number	S_t	0.37
Melt mobility number[1]	δ	10^{1}-10^{-3}
Compaction viscosity	ζ	1
Dimensionless parameters (2D DNS)		
Solid-state Rayleigh	Ra	10^{6}
Liquid-state Rayleigh	-	10^{9}
Solid-liquid viscosity contrast	-	10^{3}
Depth-dependent isochemical density contrast	R_p	11.15 – 0.823
Depth-dependent compositional density contrast	R_c	4.15 – 12.34
Stefan number	S_t	0.37
Melt mobility number[1]	δ	20×10^{-3}
Compaction viscosity	ζ	1

Table S1 Parameters used in the mutliphase flow simulations. The momentum conservation equations associated to the dimensionless numbers can be found in [3]. Due to uncertainties associated to silicate melting temperature at extremely high pressure, *i.e.*, above 200 GPa, we consider here an Earth-sized lava planet. This choice prevents the use of arbitrary parameterization of melting curves and chemical density contrasts at more extreme pressures occurring in larger planets. [1] Crystal size is captured by the dimensionless melt mobility number. A melt mobility number value of 20×10^{-3} for a Rayleigh number of 10^{6} allows to explore a geodynamic regime where solid-liquid phase separation is efficient, generating a compositional evolution [3]). Dimensionless values are constrained by current computational limitations. For instance, a realistic solid-liquid viscosity contrast is currently out of reach in this kind of fluid dynamics simulations.

Parameters	Symbol (unit)	Value
Gravitational acceleration	g ($\mathrm{m\,s^{-2}}$)	20
Rotation period	T_Ω (hours)	6 to 18
Rotation rate	$\Omega = 2\pi/(T_\Omega \times 3600)$ ($\mathrm{s^{-1}}$)	9.7×10^{-5} to 2.9×10^{-4}
Magma ocean density	ρ ($\mathrm{kg\,m^{-3}}$)	8500
Dynamic viscosity[a]	η ($\mathrm{Pa\,s}$)	1×10^{-2}
Kinematic viscosity	$\nu = \eta/\rho$ ($\mathrm{m^2\,s^{-1}}$)	1.18×10^{-6}
Thermal diffusivity	κ ($\mathrm{m^2\,s^{-1}}$)	1×10^{-6}
Thermal expansion coefficient	α ($\mathrm{K^{-1}}$)	3×10^{-5} to 10×10^{-5}
Magma Ocean thickness	D (km)	5,000
Planet radius	r_o (km)	10,000
Average super-adiabatic vertical temperature difference	ΔT (K)	1350
Maximum super-adiabatic vertical temperature difference (Night-side)	ΔT_{max} (K)	2700
Minimum super-adiabatic vertical temperature difference (Day-side)	ΔT_{min} (K)	0
Dimensionless parameters (Lava Planet)		
Aspect ratio	$1 - D/r_o$	0.5
Prandtl[a]	$Pr = \nu/\kappa$	1.18
Rayleigh	$Ra = \alpha g \Delta T D^3/(\nu\kappa)$	8.6×10^{31} to 2.9×10^{32}
Ekman	$E = \nu/(\Omega D^2)$	1.6×10^{-16} to 4.9×10^{-16}
Convective Rossby[a]	$Ro_c = \sqrt{Ra/PrE}$	1.4 to 7.6
Dimensionless parameters (3D DNS)		
Aspect ratio		0.5
Prandtl	Pr	1
Rayleigh	Ra	1.1×10^{8}
Ekman	E	∞ (non-rotating) 1.5×10^{-4} (rotating)
Convective Rossby	Ro_c	∞ (non-rotating) 1.6 (rotating)

Table S2 Physical parameters [4–6] for global magma oceans of lava planets and corresponding dimensionless parameters. Here, we assume a fully-molten, low-viscosity scenario ([a]). Parameters range are considered to illustrate the sensitivity of the convective Rossby number. Dimensionless parameters used in the 3D Direct Numerical Simulations (DNS) are provided for comparison. Lava planets Rayleigh and Ekman numbers are out-of-reach of DNS, but a realistic convective Rossby number can be obtained to ensure a correct force balance between buoyancy and rotation. The rotating simulations fall in the transitional regime of Ref.[7].

presence of rotation and turbulence, our 3D simulations confirm that the mean circulation pattern obtained in the 2D simulations is robust: a downwelling occur on the night-side, and a broad region of upwelling on the day-side. This degree-one pattern is reproduced in our 2D Cartesian simulations in the fully molten state before solidification starts.

DNS velocities

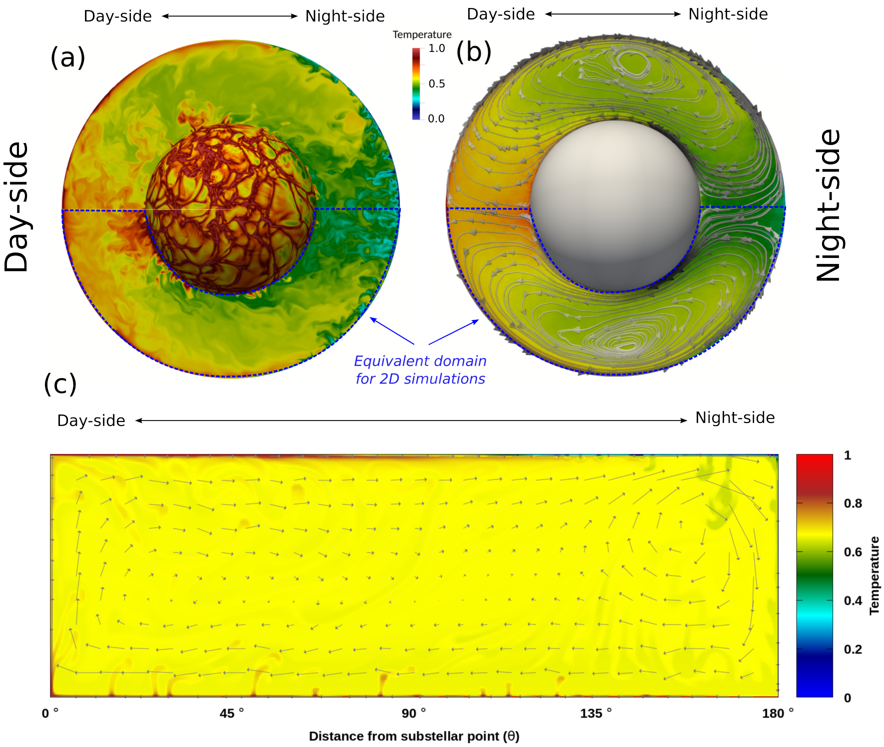

Fig. S3 Comparison of 2D Cartesian and 3D spherical simulations with no rotation. The temperature scale is the maximum super-adiabatic temperature contrast: temperature is 1 at the base of the magma ocean, 0 at the surface on the night-side and 1 at the surface on the day-side. (a) Snapshot of the temperature field in 3D spherical simulations. (b) Time-averaged temperature field and streamlines in the 3D spherical simulations. (c) Snapshot of the temperature field in the 2D Cartesian simulations.

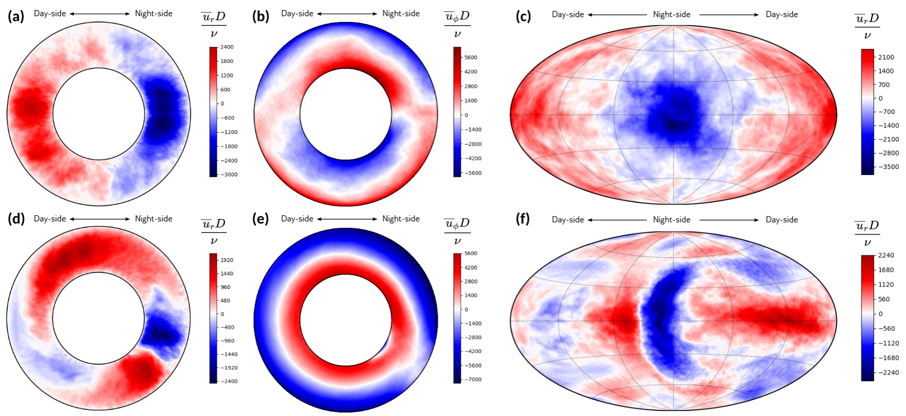

Fig. S4 Time-averaged radial ($\overline{u}_r$) and azimuthal ($\overline{u}_\phi$) velocities in the DNS. (a-c) Non-rotating DNS. (d-f) Rotating DNS. (a,b,d,e) Equatorial planes. (c,f) Hammer projection of radial velocity at mid-depth in the magma ocean.

References

[1] Nabiei, F. *et al.* Investigating magma ocean solidification on earth through laser-heated diamond anvil cell experiments. *Geophysical Research Letters* e2021GL092446 (2021) .

[2] Boukaré, C.-E., Ricard, Y. & Fiquet, G. Thermodynamics of the MgO-FeO-SiO_2 system up to 140 GPa: Application to the crystallization of Earth's magma ocean. *J Geophys. Res.: Solid Earth* **120** (9), 6085–6101 (2015). URL http://dx.doi.org/10.1002/2015JB011929. https://doi.org/10.1002/2015JB011929, 2015JB011929 .

[3] Boukaré, C.-E. & Ricard, Y. Modeling phase separation and phase change for magma ocean solidification dynamics. *Geochemistry, Geophysics, Geosystems* **18** (9), 3385–3404 (2017) .

[4] Barragán, O. *et al.* K2-141 b. A 5-$M_\oplus$ super-Earth transiting a K7 V star every 6.7 h. *Astronomy and Astrophysics* **612**, A95 (2018). https://doi.org/10.1051/0004-6361/201732217, arXiv:1711.02097 [astro-ph.EP].

[5] Batalha, N. M. *et al.* Kepler's first rocky planet: Kepler-10b. *The Astrophysical Journal* **729** (1), 27 (2011). URL http://stacks.iop.org/0004-637X/729/i=1/a=27 .

[6] Solomatov, V. S. in *Fluid Dynamics of a Terrestrial Magma Ocean* (eds Canup, R. M., Righter, K. & et al.) *Origin of the Earth and Moon* 323–338 (The University of Arizona Press, 2000).

[7] Gastine, T., Wicht, J. & Aubert, J. Scaling regimes in spherical shell rotating convection. *Journal of Fluid Mechanics* **808**, 690–732 (2016) .

[8] Maas, C. & Hansen, U. Effects of earth's rotation on the early differentiation of a terrestrial magma ocean. *Journal of Geophysical Research: Solid Earth* **120** (11), 7508–7525 (2015). URL http:https://dx.doi.org/10.1002/2015JB012053. https://doi.org/10.1002/2015JB012053 .

[9] Maas, C. & Hansen, U. Dynamics of a terrestrial magma ocean under planetary rotation: A study in spherical geometry. *Earth and Planetary Science Letters* **513**, 81–94 (2019) .